Acta Crystallographica Section D
Biological Crystallography
ISSN 1399-0047

High-resolution structures of mutants of residues that affect access to the ligand-binding cavity of human lipocalin-type prostaglandin D synthase

Massimiliano Perduca,[a]‡ Michele Bovi,[a]‡ Mattia Bertinelli,[a] Edoardo Bertini,[a] Laura Destefanis,[a] Maria E. Carrizo,[b] Stefano Capaldi[a] and Hugo L. Monaco[a]*

[a]Biocrystallography Laboratory, Department of Biotechnology, University of Verona, Strada Le Grazie 15, 37134 Verona, Italy, and [b]Departamento de Química Biológica, Facultad de Ciencias Químicas, Universidad Nacional de Córdoba, CP 5016, Córdoba, Argentina

‡ These authors contributed equally to this work.

Correspondence e-mail: monaco@sci.univr.it

Received 14 February 2014
Accepted 28 May 2014

PDB references: human L-PGDS, C65A mutant, 4orr; 4ors; 4oru; C65A/K59A mutant, 4orw; 4orx; 4ory; C65A/W54F mutant, 4os0; C65A/W112F mutant, 4os3; C65A/W54F/W112F mutant, 4os8

Lipocalin-type prostaglandin D synthase (L-PGDS) catalyzes the isomerization of the 9,11-endoperoxide group of PGH_2 (prostaglandin H_2) to produce PGD_2 (prostaglandin D_2) with 9-hydroxy and 11-keto groups. The product of the reaction, PGD_2, is the precursor of several metabolites involved in many regulatory events. L-PGDS, the first member of the important lipocalin family to be recognized as an enzyme, is also able to bind and transport small hydrophobic molecules and was formerly known as β-trace protein, the second most abundant protein in human cerebrospinal fluid. Previous structural work on the mouse and human proteins has focused on the identification of the amino acids responsible and the proposal of a mechanism for catalysis. In this paper, the X-ray structures of the apo and holo forms (bound to PEG) of the C65A mutant of human L-PGDS at 1.40 Å resolution and of the double mutant C65A/K59A at 1.60 Å resolution are reported. The apo forms of the double mutants C65A/W54F and C65A/W112F and the triple mutant C65A/W54F/W112F have also been studied. Mutation of the lysine residue does not seem to affect the binding of PEG to the ligand-binding cavity, and mutation of a single or both tryptophans appears to have the same effect on the position of these two aromatic residues at the entrance to the cavity. A solvent molecule has also been identified in an invariant position in the cavity of virtually all of the molecules present in the nine asymmetric units of the crystals that have been examined. Taken together, these observations indicate that the residues that have been mutated indeed appear to play a role in the entrance–exit process of the substrate and/or other ligands into/out of the binding cavity of the lipocalin.

1. Introduction

The enzyme prostaglandin D synthase (or prostaglandin-H_2 D-isomerase; PGDS; EC 5.3.99.2) catalyzes the isomerization of the 9,11-endoperoxide group of PGH_2 (prostaglandin H_2) to produce PGD_2 (prostaglandin D_2) with 9-hydroxy and 11-keto groups. PGH_2, its substrate, is a common precursor of all prostanoids, which include thromboxanes, prostacyclins and prostaglandins, whereas the product PGD_2 is the precursor of several metabolites involved in many regulatory events.

Two types of prostaglandin D synthase have been characterized: haematopoietic PGDS (H-PGDS; Kanaoka & Urade, 2003), which requires the cofactor glutathione (a

tripeptide γ-glutamylcysteinyl glycine in which the thiol group of cysteine is responsible for the biological activity), and glutathione-independent or lipocalin-type PGDS (L-PGDS; Urade & Hayaishi, 2000; Urade & Eguchi, 2002).

H-PGDS is a cytosolic enzyme whose highest levels of expression are observed in spleen and bone marrow, in mast cells, antigen-presenting cells and Th2 cells. It is the only mammalian member of the sigma class of cytosolic glutathione *S*-transferases (Flanagan & Smythe, 2011) and participates in allergic and inflammatory reactions (Jowsey *et al.*, 2001). Its three-dimensional X-ray structure has been determined (Kanaoka *et al.*, 1997) and the amino-acid residues involved in catalysis have been identified (Pinzar *et al.*, 2000).

L-PGDS, the first member of the important lipocalin family to be recognized as an enzyme (Peitsch & Boguski, 1991), is also able to bind and transport small hydrophobic molecules including biliverdin, bilirubin, thyroid hormone (Beuckmann *et al.*, 1999), retinal and retinoic acid (Tanaka *et al.*, 1997) and may act as a scavenger for harmful hydrophobic ligands. A systematic analysis of the interaction of hydrophobic ligands with L-PGDS has been carried out using tryptophan fluorescence quenching, induced circular dichroism and isothermal titration calorimetry (Kume *et al.*, 2012). The enzyme was formerly known as β-trace protein (Kuruvilla *et al.*, 1991; Hoffmann *et al.*, 1993), the second most abundant protein in human cerebrospinal fluid, although it is also detected in brain, testis and prostate, endothelial cells, placenta and heart tissue and in macrophages infiltrated in atherosclerotic plaques (Tanaka *et al.*, 2009).

L-PGDS is involved in a variety of CNS functions such as NREM (nonrapid eye movement) sleep (Jordan *et al.*, 2004; Qu *et al.*, 2006) and allodynia, *i.e.* the perception of pain owing to innocuous stimuli which do not normally evoke it (Eguchi *et al.*, 1999). It also appears to be a major endogenous amyloid β-chaperone in human cerebrospinal fluid and in the brain and thus it has been suggested that disturbance of this function may be involved in the onset and progression of Alzheimer's disease (Kanekiyo *et al.*, 2007). In general, it is believed to play key roles in both the maturation and the maintenance of the central nervous system and the male reproductive system (Beuckmann *et al.*, 2000; Samy *et al.*, 2000). It is also overexpressed in the bald scalp of men with androgenic alopecia (Garza *et al.*, 2012) and is used clinically as a diagnostic marker for liquorrhoea, that is the outflow of cerebrospinal fluid leaking from the nose or ear (Bachmann *et al.*, 2002).

NMR studies on mouse L-PGDS have established that the protein indeed belongs to the lipocalin family (Shimamoto *et al.*, 2007) and X-ray structural work using crystals of the C65A mutant, grown in the presence of retinoic acid as an essential additive for crystallization, confirmed that the overall structure of the core region of the β-barrel in the crystals was essentially identical to that in solution. Two conformers were identified in the X-ray work: one with the central cavity open and the other with the cavity closed. The large central cavity of L-PGDS was found to be separated into two compartments by several hydrophobic amino acids, with Cys65, which is known to be essential for catalytic activity (Urade *et al.*, 1995), located in the upper compartment of the cavity (Kumasaka *et al.*, 2009). Structural studies on crystals of the C65A mutant of human L-PGDS complexed with bound fatty acids further explored the mode of ligand binding to the enzyme (Zhou *et al.*, 2010). Wild-type human L-PGDS was also crystallized and studied by X-ray diffraction and the catalytic Cys65 thiol group was found in two different conformations. Although one of the crystal forms had been crystallized in the presence of a substrate analogue, the electron density for the ligand observed in the active site could only be used to define the substrate-binding region of the enzyme; it did not allow the unambiguous fitting of the ligand in a single position (Lim *et al.*, 2013).

In the previous X-ray diffraction crystallographic work, attention was focused on amino acids presumed to be involved in catalysis. Here, we present studies of mutants of residues of human L-PGDS that are believed to play a role in the entrance/exit of the ligands to/from the central binding cavity.

Table 1
Primers used in the construction of the mutants.

The primers in the right-hand column introduce the mutation in bold in the left-hand column.

Mutant	Primers
C65A	for: GCGTTGTCCATG**GCC**AAGTCTGTGGTG
	rev: CACCACAGACTT**GGC**CATGGACAACGC
C65A/**K59A**	(C65A) +
	for: CTCCGGGAGAAG**GCC**GCGGCGTTGTCC
	rev: GGACAACGCCGC**GGC**CTTCTCCCGGAG
C65A/**W54F**	(C65A) +
	for: TCCAACTCGAGC**TTC**CTCCGGGAGAAG
	rev: CTTCTCCCGGAG**GAA**GCTCGAGTTGGA
C65A/**W112F**	(C65A) +
	for: CGGAGTCCCCAC**TTC**GGCAGCACCTAC
	rev: GTAGGTGCTGCC**GAA**GTGGGGACTCCG
C65A/W54F/**W112F**	(C65A/W54F) +
	for: CGGAGTCCCCAC**TTC**GGCAGCACCTAC
	rev: GTAGGTGCTGCC**GAA**GTGGGGACTCCG

2. Materials and methods

2.1. Construction of the mutants

The cDNA coding for human lipocalin-type prostaglandin D synthase (L-PGDS; Image ID 4294999), obtained from RZPD (Deutsches Ressourcenzentrum für Genomforschung GmbH), was amplified by PCR using primers designed to exclude the 22-amino-acid N-terminal signal peptide. The PCR product and the expression vector pTYB1 (New England Biolabs) were digested with the enzymes *Nde*I and *Sap*I and were incubated with ligase to insert the cDNA into the vector respecting the open reading frame. The vector pTYB1 expresses the protein fused to the C-terminus of an intein/chitin-binding domain tag, which is useful for the purification of the protein because the binding domain interacts with chitin and intein self-cleaves in the presence of reducing thiols.

Site-directed mutagenesis to produce the C65A mutant was performed by PCR using the QuikChange II site-directed mutagenesis kit (Stratagene) with the wild-type construct as a template. The mutant vector was then used as a template to

prepare the subsequent mutants. The primers used to introduce all of the desired mutations are listed in Table 1. The recombinant DNAs were fully sequenced to confirm the planned mutation and to ascertain that no spurious mutations had occurred.

2.2. Overexpression and purification of the proteins

For the L-PGDS C65A and C65A/K59A mutants the following protocol was used. BL21 (DE3) strain *Escherichia coli* cells were transformed by heat shock with the resulting vectors and grown in LB medium at 37°C until an OD_{600} of 0.8 was reached; protein synthesis was then induced overnight at 20°C with 0.25 m*M* IPTG (isopropyl β-D-1-thiogalactopyranoside).

The bacterial cells were recovered by centrifugation at 8000*g* for 10 min and resuspended in 20 m*M* Tris–HCl pH 7.5, 0.5 *M* NaCl, 1 m*M* EDTA for sonication. After centrifugation at 10 000*g* for 10 min to remove debris, the soluble fraction was loaded onto a chitin column equilibrated with the same buffer. The presence of the intein tag allowed affinity purification of the fused proteins by passing the bacterial extracts through a chitin column. After extensive washing with 20 m*M* Tris–HCl pH 7.5, 1.0 *M* NaCl, 0.2% Tween 20 to remove impurities, the column was equilibrated with 20 m*M* Tris–HCl pH 7.5, 0.5 *M* NaCl, 1 m*M* EDTA, 10 m*M* DTT and left at 20°C overnight to allow intein cleavage. The eluted protein in 20 m*M* Tris–HCl pH 7.5, 0.5 *M* NaCl, 1 m*M* EDTA was further purified by size-exclusion chromatography on a Superdex G-75 (Pharmacia) column and by hydrophobic interaction chromatography using Lipidex 1000 resin in a column thermostated at 37°C.

For the L-PGDS C65A/W54F, C65A/W112F and C65A/W54F/W112F mutants a different protocol was used.

The mutants were prepared by inserting the mutated C65A template into the pGEX4T-1 plasmid, which expresses the protein with its N-terminus fused to glutathione *S*-transferase (GST) through a thrombin-cleavage site. The recombinant GST-fusion protein can be purified directly from the pre-treated cell lysate by using a glutathione (GSH) Sepharose resin. The tag-free target protein can then be recovered from the column by digestion with thrombin followed by elution with a standard buffer.

For protein expression the same BL21 (DE3) *E. coli* strain and identical cell-growth and cell pre-treatment conditions were used. The supernatant was loaded onto a GSH Sepharose column previously equilibrated with 20 m*M* Tris–HCl pH 7.5, 0.5 *M* NaCl; after eliminating the contaminants, 30 units of thrombin were added to the column, which was left to react overnight at 20°C. The L-PGDS double and triple mutants were recovered from the column with the Tris buffer and further loaded onto a GSH Sepharose column to remove traces of the chimeric uncleaved protein. A final step of hydrophobic interaction chromatography using Lipidex1000 resin was also carried out for the double mutants.

The protein concentrations were determined from the specific extinction coefficient at 280 nm and the purity and molecular weight were assessed by SDS–PAGE with standard molecular-weight markers.

Table 2
Crystallization conditions.

Unit-cell parameters and data-collection statistics are given in Table 3.

Crystal form	Mutant	Space group	Reservoir solution
1	C65A	$P6_122$	0.1 *M* Tris pH 7.0, 25% PEG 4000, 2% ethylene glycol
2	C65A	*P*1	0.1 *M* Na HEPES pH 7.5, 2% PEG 400, 2.0 *M* ammonium sulfate
3	C65A	$P4_1$	30% PEG 4000, 0.2 *M* ammonium sulfate pH 4.1
4	C65A/K59A	$P2_12_12_1$	0.1 *M* Tris pH 8.5, 2.0 *M* ammonium phosphate
5	C65A/K59A	$P4_1$	30% PEG 4000, 0.2 *M* ammonium sulfate pH 4.1
6	C65A/K59A	$P4_1$	0.1 *M* sodium acetate pH 4.6, 0.2 *M* ammonium sulfate, 30% PEG 2000 monomethyl ether
7	C65A/W54F	*P*1	0.2 *M* potassium sodium tartrate, 0.1 *M* sodium acetate pH 5.6, 2.0 *M* ammonium sulfate
8	C65A/W112F	*P*1	(i) 0.1 *M* sodium acetate, 2.0 *M* ammonium sulfate pH 4.6 (ii) 2.0 *M* ammonium sulfate pH 5.9 (iii) 0.2 *M* potassium sodium tartrate, 0.1 *M* sodium acetate pH 5.6, 2.0 *M* ammonium sulfate
9	C65A/W54F/W112F	*P*1	0.1 *M* sodium acetate, 2.0 *M* ammonium sulfate pH 4.6

2.3. Crystallization

The purified proteins were used at a concentration of about 25 mg ml^{-1} for initial screening of crystallization conditions. Molecular Dimensions Structure Screens were employed at 20°C with the hanging-drop method, mixing 1 µl protein solution (in 150 m*M* NaCl, 20 m*M* Tris–HCl buffer pH 7.5) with the same volume of precipitating solution and equilibrating against a volume of 0.3 ml of the latter in the reservoir. The conditions yielding small crystals were later refined and the sitting-drop method with larger volumes was also tested until crystals that were large enough for data collection were obtained. The precipitating solutions that yielded crystals suitable for X-ray diffraction are listed in Table 2. Diffraction-quality crystals were obtained in about 4–5 d at 20°C.

2.4. Data collection and processing

Preliminary data were collected on a MAR345 image plate using radiation produced by a Rigaku RU-300 rotating-anode X-ray generator. The incident X-ray beam was focused with Xenocs multilayer confocal mirrors that selected Cu $K\alpha$ radiation. The final data used for refinement were collected on various beamlines at the European Synchrotron Radiation Facility (ESRF) in Grenoble. The diffraction data were collected from crystals cooled to 100 K after brief immersion into a mixture of 70% mother liquor and 30% glycerol. The data were indexed, integrated and reduced using *MOSFLM* (Leslie & Powell, 2007) and *SCALA* (Evans, 2006). The

Table 3
Data-collection and refinement statistics.

Values in parentheses are for the highest resolution shell.

Data set	C65A	C65A	C65A	C65A/K59A	C65A/K59A	C65A/K59A	C65A/W54F	C65A/W112F	C65A/W54F/W112F
Space group	$P6_122$	$P1$	$P4_1$	$P2_12_12_1$	$P4_1$	$P4_1$	$P1$	$P1$	$P1$
Crystal form	1	2	3	4	5	6	7	8	9
Unit-cell parameters									
a (Å)	60.78	43.13	91.13	38.33	90.97	67.38	41.62	42.25	42.51
b (Å)	60.78	45.82	91.13	57.63	90.97	67.38	45.87	46.25	46.62
c (Å)	178.77	49.15	36.81	131.80	36.74	287.67	48.26	47.78	47.89
α (°)	90.0	73.12	90.0	90.0	90.0	90.0	69.40	68.89	69.14
β (°)	90.0	82.82	90.0	90.0	90.0	90.0	77.67	77.15	77.10
γ (°)	120	64.90	90.0	90.0	90.0	90.0	65.32	65.17	64.81
Molecules in the asymmetric unit	1	2	2	2	2	8	2	2	2
Resolution range (Å)	30.0–1.40	40.03–1.40	45.56–1.55	57.63–1.66	28.77–1.60	50.0–1.80	45.04–1.75	26.08–1.40	33.73–1.69
Observed reflections	743727	129614	176101	140796	293569	481238	104994	226240	74160
Independent reflections	39501	60070	44187	34796	39985	117470	29286	57481	33458
Multiplicity	18.8 (12.8)	2.2 (2.2)	4.0 (3.9)	4.0 (4.2)	7.3 (7.2)	4.1 (4.1)	3.6 (3.6)	3.9 (3.9)	2.2 (2.1)
$R_{\rm merge}$† (%)	6.6 (32.1)	11.8 (33.4)	4.3 (35.4)	6.0 (35.3)	5.8 (30.9)	7.0 (6.1)	6.7 (35.2)	3.1 (38.3)	9.0 (20.5)
$\langle I/\sigma(I)\rangle$	32.2 (6.4)	8.0 (2.1)	13.8 (3.3)	13.0 (3.7)	18.8 (5.9)	11.2 (2.6)	10.0 (3.4)	13.2 (3.5)	9.6 (5.0)
Completeness (%)	99.8 (99.7)	93.5 (91.9)	99.6 (99.7)	99.1 (99.4)	99.7 (100)	99.6 (100.0)	95.9 (95.0)	95.7 (94.4)	96.3 (94.8)
Reflections in refinement	39409	60070	44155	34739	39967	117341	29212	57479	33458
$R_{\rm cryst}$‡ (%)	21.41	24.98	20.82	20.13	19.88	20.79	19.58	22.06	19.43
$R_{\rm free}$§ (%)	23.27	27.99	23.49	23.98	22.61	24.89	23.28	24.56	23.24
Protein atoms	1262	2546	2492	2482	2482	10044	2548	2540	2534
Ligand atoms	45	5	76		81	152			
Water molecules	102	192	84	120	106	142	105	87	135
R.m.s.d.¶									
Bond lengths (Å)	0.004	0.005	0.004	0.004	0.004	0.005	0.004	0.008	0.004
Bond angles (°)	1.012	0.871	0.886	0.903	0.922	1.014	0.944	1.190	0.903
Planar groups (Å)	0.004	0.004	0.003	0.003	0.003	0.004	0.004	0.007	0.004
Chiral volumes (Å^3)	0.033	0.062	0.063	0.062	0.063	0.070	0.068	0.082	0.065
Average B factor (Å^2)									
Overall	22.31	17.00	28.60	19.59	25.75	43.25	39.00	25.30	14.23
Protein atoms	21.39	16.71	28.17	19.55	25.02	43.09	39.02	25.25	14.17
Ligand atoms	34.20	12.57	42.93		46.33	64.28			
Solvent atoms	28.46	20.87	28.45	20.39	27.29	32.36	38.52	26.85	15.42
PDB code	4orr	4ors	4oru	4orw	4orx	4ory	4os0	4os3	4os8

† $R_{\rm merge} = \sum_{hkl}\sum_i |I_i(hkl) - \langle I(hkl)\rangle|/\sum_{hkl}\sum_i I_i(hkl)$, where $\langle I(hkl)\rangle$ is the mean intensity of the i observations of reflection hkl. ‡ $R_{\rm cryst} = \sum_{hkl}\big||F_{\rm obs}| - |F_{\rm calc}|\big|/\sum_{hkl}|F_{\rm obs}|$, where $|F_{\rm obs}|$ and $|F_{\rm calc}|$ are the observed and calculated structure-factor amplitudes, respectively. Summation includes all reflections used in the refinement. § $R_{\rm free} = \sum_{hkl}\big||F_{\rm obs}| - |F_{\rm calc}|\big|/\sum_{hkl}|F_{\rm obs}|$ evaluated for a randomly chosen subset of 5% of the diffraction data not included in the refinement. ¶ Root-mean-square deviation from ideal values.

processed data were converted to structure factors using *TRUNCATE* from the *CCP*4 suite (Winn *et al.*, 2011).

A summary of the data-collection statistics is given in Table 3.

2.5. Structure determination and refinement

The structure of the C65A mutant in the $P6_122$ crystal form was solved using the molecular-replacement method as implemented in *MOLREP* (Vagin & Teplyakov, 2010). The search probe used was monomer *A* of the complex of L-PGDS with fatty acids, but with the ligands removed, solved at 1.7 Å resolution (Zhou *et al.*, 2010; PDB entry 3o2y). The rotation function gave an unambiguous answer with an Rf/σ coefficient of 6.48. The highest peak of the translation function had a Tf/σ of 22.52, a score of 61.8 and an R factor of 54.1 for the data in the 29.6–1.7 Å resolution interval. Examination of the molecular packing in the unit cell after rigid-body refinement showed that there were no clashes with the symmetry-related molecules in this space group and confirmed that the search model was indeed properly oriented and positioned in the unit cell. The C65A mutant in space group $P1$, the C65A mutant in space group $P4_1$, the C65A/K59A double mutant in space group $P2_12_12_1$ and the octameric form of the C65A/K59A double mutant in space group $P4_1$ were all solved by molecular replacement using the refined coordinates of the C65A mutant model in space group $P6_122$ as the search probe. All of the other crystal forms listed in Table 3 are isomorphous to a solved structure and therefore difference Fourier maps were calculated directly with the experimental data and the phases of the solved structure.

The initial models were first refined by simulated annealing using *phenix.refine* (Afonine *et al.*, 2005; Davis *et al.*, 2007) from the *PHENIX* suite (Adams *et al.*, 2010). The next step was a series of several rounds of positional refinement alternated with manual model revision using *Coot* (Emsley *et al.*, 2010) and the refinement programs *REFMAC* (Murshudov *et al.*, 2011) and *phenix.refine*. During the process of refinement and model building the quality of the models was controlled using *PROCHECK* (Laskowski *et al.*, 1993).

The models were finally subjected to final rounds of TLS and anisotropic refinement. The ligands in the crystals were modelled into difference Fourier maps phased by the refined unliganded structures. Solvent molecules were added to the

models in the final stages of refinement according to hydrogen-bond criteria and only if their B factors refined to reasonable values and if they improved the R_{free}.

The diffraction data and refinement statistics of all of the models are summarized in Table 3. The final R factors and r.m.s. deviations in Table 3 were calculated with *phenix.refine* (Afonine *et al.*, 2005; Davis *et al.*, 2007).

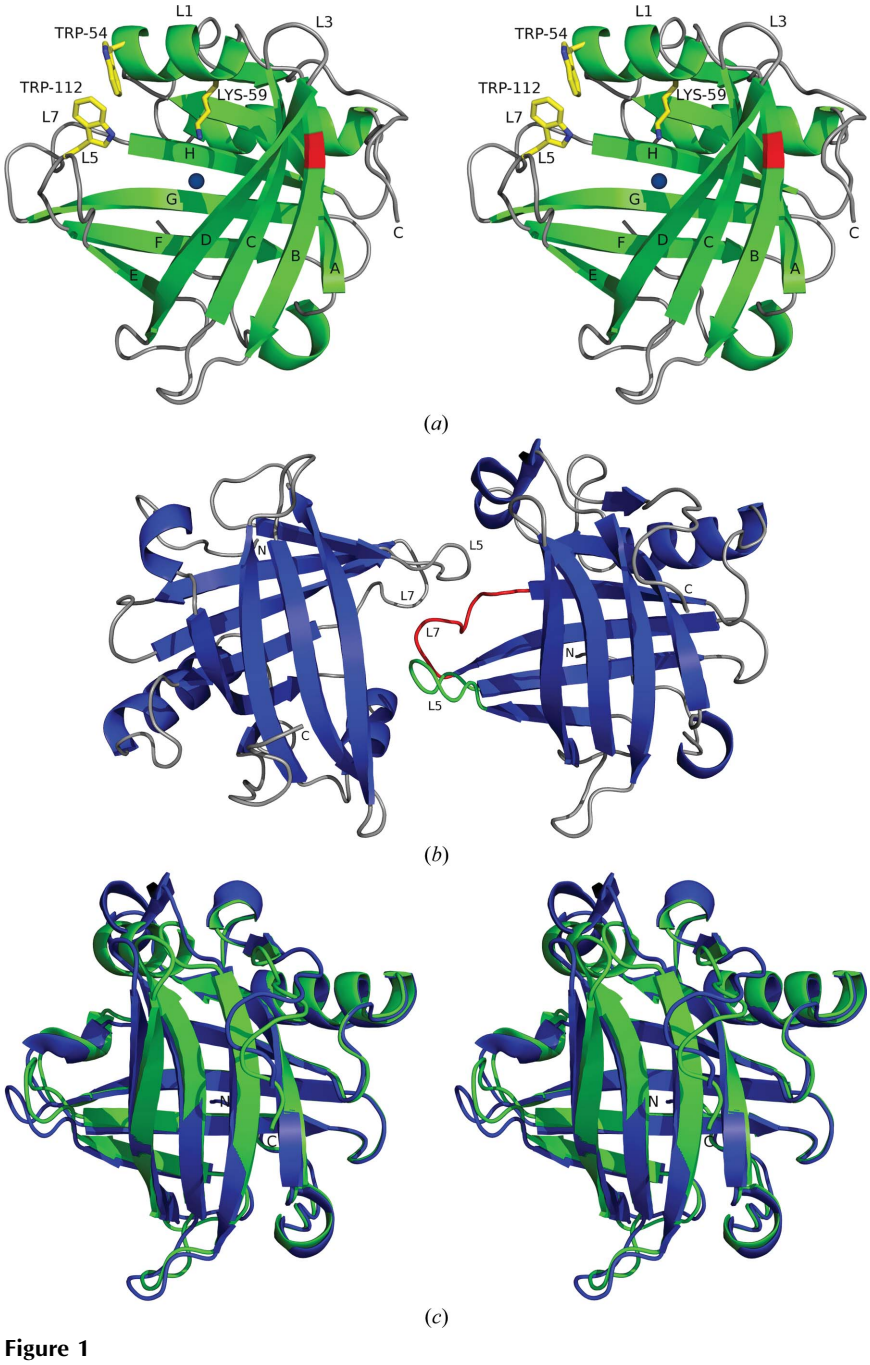

Figure 1
Apo and holo crystals of the C65A mutant of human L-PGDS. (*a*) Stereo diagram representing a human L-PGDS monomer. The figure was prepared with the coordinates of crystal form 1 (L-PGDS bound to PEG). The eight strands of the β-sheet are identified with the letters A–H and the position of the active-site Cys65 is indicated in red. The side chains of the mutated amino acids are represented in yellow and blue and the blue dot identifies the position of the conserved water molecule. Only the four loops at the entrance of the barrel are indicated in the figure: L1, A–B; L3, C–D; L5, E–F; L7, G–H. Note the presence of the helix in the first loop L1. (*b*) The asymmetric unit of the apo form of the C65A mutant, crystal form 2. In the figure the loops L5 and L7 of monomer *A* are coloured green and red, respectively. (*c*) Stereoview of the unliganded monomer *A* of crystal form 2 of the C65A mutant of human L-PGDS and the mutant bound to PEG in crystal form 1. The apo form of the protein is in blue and the molecule with PEG in the cavity is in green. Note the important difference in the first helix of loop L1.

2.6. Fluorometric titrations

All measurements were conducted with an FP 8200 spectrofluorometer (Jasco, Easton, Maryland, USA) with the samples at room temperature. L-PGDS (1 µ*M*) in 20 m*M* Tris–HCl pH 7.5 buffer was titrated with 0.5 µl injections of the crystallization solution of crystal form 3 consisting of 0.2 *M* ammonium sulfate, 30%(*w*/*v*) PEG 4000. Fluorescence emission spectra were acquired with 5 nm width excitation and emission slits. The excitation wavelength was 295 nm and emission was recorded in the 305–500 nm range. Data were analyzed using *SigmaPlot* v.9.0 (Systat Software Inc., San Jose, California, USA).

2.7. Isothermal titration calorimetry

The diluted (1:100) precipitating solution of crystal form 3 consisting of 2 m*M* ammonium sulfate, 0.3%(*w*/*v*) PEG 4000 was titrated with the protein solution. The protein was dissolved to a concentration of 9 µ*M* in 20 m*M* Tris–HCl pH 7.5, 0.15 *M* NaCl. The titrations were performed at 25°C using a Nano ITC instrument (TA Instruments, New Castle, Delaware, USA). A total of 25 injections of 2 µl aliquots of the protein titrating solution were added under stirring with 5 min intervals to the 300 µl PEG solution cell. The heat of the injections was corrected for the heat of dilution of the protein into the PEG solution. Three replicates were performed. The data were analyzed using *NanoAnalyze* (TA Instruments, New Castle, Delaware, USA).

2.8. Analysis of the models

The superposition of the models matching the secondary structure was performed using the *SSM Superposition* subroutine of *Coot* (Krissinel & Henrick, 2004). The distances between the ligand, PEG and protein atoms were calculated with the *CCP*4 program *CONTACT* (Tadeusz Skarzynski, Imperial College, London). Structurally invariant water molecules were identified using the web-based program 3*d-SS* (http://cluster.physics.iisc.ernet.in/3dss/; Sumathi *et al.*, 2006). Figures of the

structures were prepared and rendered with *PyMOL* (http://www.pymol.org).

3. Results

3.1. General features of the structures

As expected, all of the mutants present the classical lipocalin fold. We have chosen crystal form 1, *i.e.* a crystal of the C65A mutant, which was the first structure that we solved, diffracts to 1.4 Å resolution and contains one molecule in the asymmetric unit, to define the secondary-structure elements. The final L-PGDS model in this crystal form spans the sequence from Val28 to Thr188. In the current standard notation that we use residues 1–22 are the signal peptide, so the mature polypeptide chain spans residues 23–190. The model includes 1262 protein atoms, one sulfate, a PEG molecule and 102 water molecules. No clear electron density is present for the first five and the last two residues, and partially disordered regions with discontinuous electron density are found between Ala72 and Gly75 and between Arg85 and Gln88. The conventional *R* factor for all data to a resolution of 1.40 Å is 21.3% and the free *R* factor is 23.2% (Table 3). 91.5% of the residues are in the most favourable region of the Ramachandran plot and 7.1% are in the additionally allowed region. Tyr125 and Ser114 are in disallowed regions of the plot. An equivalent of the first of these two amino acids is typically found in disallowed regions in lipocalins, whereas the distortion in the second is probably owing to the presence of the PEG molecule bound in the crystals since it is absent in the apo form (crystal form 2) and in crystal form 3, in which the PEG molecule adopts a slightly different conformation. The overall fold consists of the canonical β-barrel with eight strands of antiparallel β-chain with a first short α-helix in the loop between strands A and B and a second longer α-helix packed against the barrel. The final secondary-structure assignments are as follows for the β-strands: strand A, residues 41–50; strand B, residues 63–71; strand C, residues 77–85; strand D, residues 88–98; strand E, residues 104–108; strand F, residues 115–123; strand G, residues 128–137; strand H, residues 144–150. The two α-helices span residues 53–60 and 157–169. In addition, a very short β-strand spanning residues 177–179 and three 3_{10}-helices spanning residues 36–39, 139–142 and 174–176 were also identified. The opening of the ligand-binding site at one end of the L-PGDS model has four loops joining strands A and B (L1), C and D (L3), E and F (L5) and G and H (L7). The other three loops (L2, L4 and L6) are at the opposite closed end of the molecule (Flower *et al.*, 2000). Fig. 1(*a*) shows a stereo diagram of the L-PGDS molecule that identifies the elements of secondary structure, Cys65 and the four loops that control access to the ligand-binding cavity.

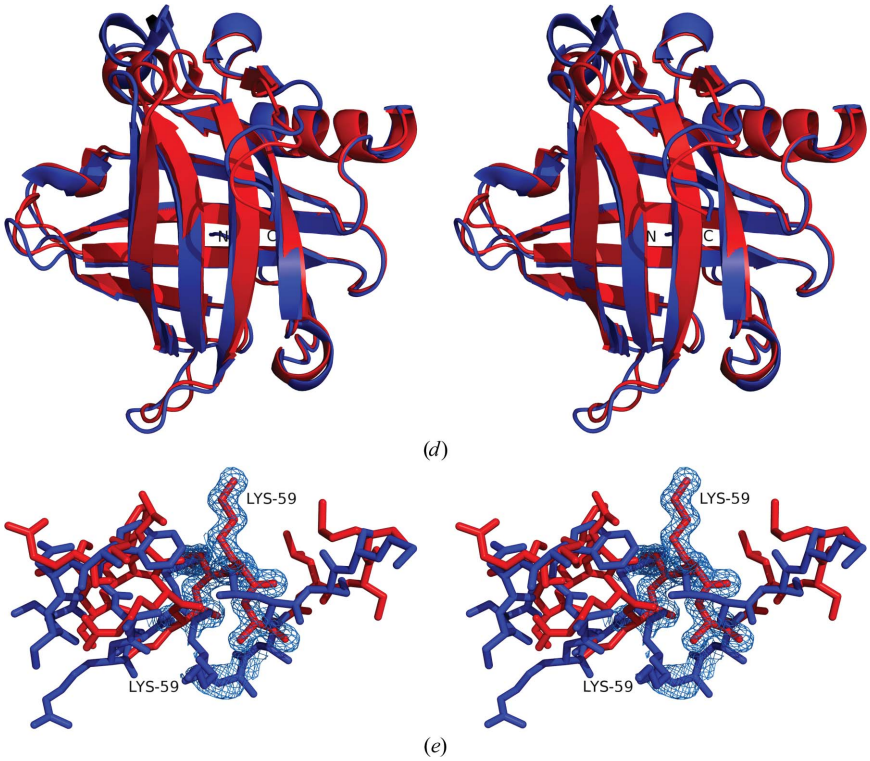

Figure 1 (continued)
(*d*) A similar stereoview in which the two models superimposed are monomer *A* of crystal form 2 and monomer *A* of crystal form 3. The apo form of the protein is again shown in blue. Note that the changes are very similar to those observed in the other crystal form. (*e*) Stereo diagram showing a superposition of the polypeptide chains spanning residues 50–64 of molecule *A* of crystal form 1 and molecule *A* of crystal form 2. The apo form of the protein is in blue and the holo form is in red. The electron density, contoured at a 1.0σ level, was represented for amino acids 58–60 of both forms. In the holo form Lys59 is vertical while in the apo form it points in the direction of the reader.

3.2. Binding of polyethylene glycol to the C65A mutant

In the structure of crystal forms 1 and 3 of the C65A mutant, a very clear and continuous electron density was found occupying the ligand-binding cavity. It was interpreted as a PEG molecule, a ligand that was also found in the cavity of this molecule by Lim *et al.* (2013). Crystal form 2, which contains two monomers in the asymmetric unit, is the apo form of this mutant. Although polyethylene glycol was also present in the mother liquor used to prepare these crystals (see Table 2), PEG did not access the ligand-binding cavity because the two monomers present in the asymmetric unit pack with loops L5 (residues 109–114) and L7 (residues 138–143) of one monomer blocking access to the cavity of the other. The inaccessibility of the cavity was confirmed by soaking experiments with these crystals. Fig. 1(*b*) shows the packing of the two monomers in the asymmetric unit of crystal form 2, in which loops L5 and L7 of monomer *A* are coloured green and red.

The two holo conformations in which L-PGDS is bound to PEG in crystal forms 1 and 3 are very similar to each other and do

not differ greatly from the apo conformation of crystal form 2. Fig. 1(*c*) shows a stereo representation of the superimposed structures of the apo form (blue) and the holo form (green) of crystal form 1 and Fig. 1(*d*) shows a similar representation with the holo form of crystal form 3 (red). In both cases the main difference is in loop L1, in which the first helix is less structured and shorter in the apo form, in which the electron density is less clear and in some sections discontinuous. As a consequence, the models of the two molecules in the asymmetric unit of the apo protein in crystal form 2 present some differences in this area, with molecule *B* being more similar to the holo form. Fig. 1(*e*) examines in detail L1, the area where the apo–holo differences are more substantial. The secondary structures of molecule *A* of crystal form 1 and molecule *A* of crystal form 2 were superimposed and the models and electron densities of the polypeptide chains spanning residues 50–64 were represented in stereo. Note the position of Lys59 in the apo and holo forms. The side chain points towards the interior of the cavity in the holo form and towards the outside in the apo form. In the other molecule of the asymmetric unit of the apo form the apo–holo differences are not as important.

Table 4
Hydrophobic contacts with PEG molecules.

	Crystal form 1	Crystal form 3	Crystal form 5	Crystal form 6
Leu48			*B*	*F*
Trp54	*A*		*A*	*E*
Leu55	*A*	*A*, *B*	*A*, *B*	*E*, *F*, *G*, *H*
Ala59				*G*
Leu62	*A*	*A*, *B*	*A*, *B*	*F*, *H*
Met64	*A*	*A*, *B*		
Leu79	*A*	*A*, *B*	*A*	*F*
Phe83	*A*	*A*, *B*		
Met94	*A*	*A*, *B*	*A*, *B*	*E*, *F*, *G*, *H*
Trp112	*A*	*A*, *B*	*A*, *B*	*E*, *F*, *G*
Val118	*A*	*A*, *B*		*E*, *F*, *G*
Phe143	*A*	*A*, *B*	*A*, *B*	*E*, *F*, *G*, *H*
Met145	*A*	*A*, *B*	*A*, *B*	*E*, *G*, *H*

The electron density assigned to PEG in crystal form 3 is very clear and extends from one molecule into the second molecule present in the asymmetric unit, thus defining a pseudo-dimer in which, although the two monomers are not exactly equivalent, an approximate noncrystallographic twofold axis is evident, as shown in Fig. 2(*a*). The molecular weight of the PEG molecule fitted to the experimental electron density is 1117, *i.e.* the model of the molecule is shorter than the most abundant species present in the crystallization mother liquor. The presence of electron density corresponding to a lower molecular-weight species could be owing to either disordered density in the crystals or to the binding of a lower molecular-weight polymer present in the crystallization

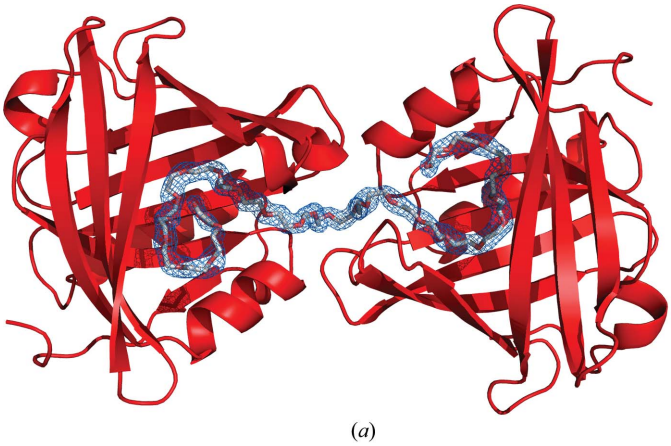

Figure 2
Binding of polyethylene glycol to the C65A mutant of human L-PGDS. (*a*) Electron density of the PEG molecule in the asymmetric unit of crystal form 3. The approximate twofold axis is perpendicular to the plane of the figure. The $2F_{obs} - F_{calc}$ map was contoured at the 1.0σ level. (*b*) Fluorometric titration of human L-PGDS with PEG. The titration curves were obtained by adding 0.5 µl injections of a 30% PEG 4000 solution to a 1 µ*M* sample of L-PGDS in 20 m*M* Tris–HCl pH 7.5. The arrow indicates the progressive quenching in arbitrary units of the maximal fluorescence emission. The inset shows the fluorescence quenching as a function of PEG 4000 concentration. (*c*) Isothermal titration calorimetry. The figure represents the titration curve obtained with 2 µl injections of a 9 µ*M* L-PGDS solution added to 300 µl of a 750 µ*M* PEG solution. The raw data are shown in the top part of the figure as a plot of corrected heat rate *versus* time. The line at the bottom represents the best fit of the data assuming a stoichiometry of two L-PGDS molecules per PEG molecule.

mother liquor or to both factors. It is worth mentioning that a very similar situation was described by Lim *et al.* (2013), who used PEG 2000 MME in the crystallization mother liquor but fitted a PEG molecule of molecular weight 250. Many hydrophobic interactions were identified in all of the crystal forms that contain PEG bound in the central cavity. They are all included in Table 4, in which the residues interacting with PEG are listed along with the molecules in which the interaction was observed. It is also worth mentioning that its electron density overlaps very well with that of the endo-

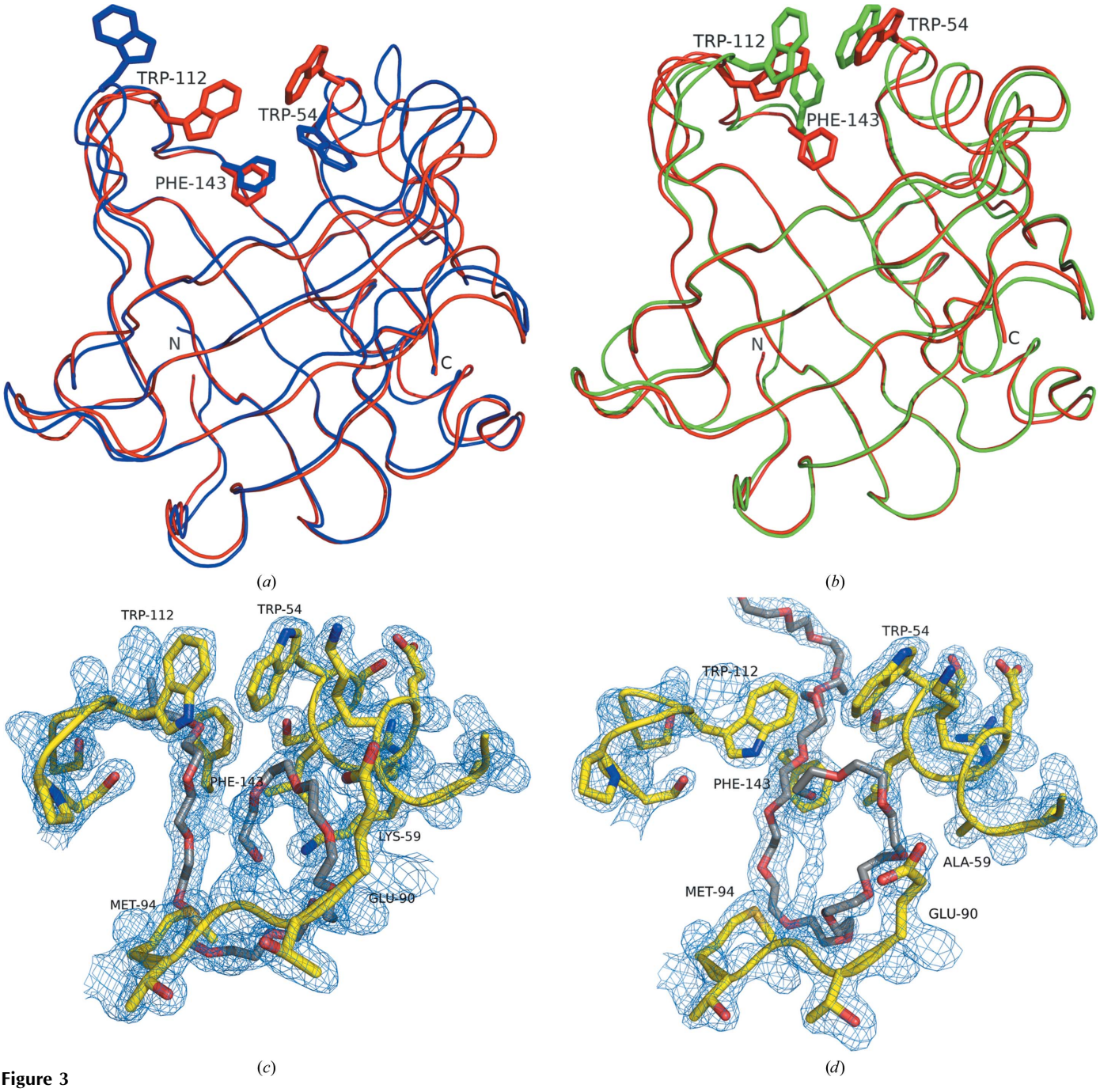

Figure 3
The C65A/K59A double mutant. (*a*) Superposition of the C_α chain trace of the apo forms of the C65A (crystal form 2) and C65A/K59A (crystal form 4) mutants. The single mutant is shown in blue and the double mutant in red. The most important differences are observed in loop L1, which contains the first α-helix, and in the position of the side chains of Trp54 and Trp112, which are not in contact in the single mutant and move closer to each other in the double mutant, approaching from a distance of about 9 Å to about 4–5 Å. (*b*) Superposition of the C_α chain trace of the L-PGDS molecule bound to PEG of the C65A (crystal form 1) and C65A/K59A mutants (crystal form 5). The single mutant is shown in green and the double mutant is again shown in red. In the double mutant the ring of Phe143 moves to occupy space vacated by the absence of the lysine side chain. (*c*) Electron density of the PEG molecule curling around the Lys59 side chain (crystal form 1). The $2F_{obs} - F_{calc}$ map was contoured at the 1.0σ level. (*d*) Binding of PEG to the double mutant C65A/K59A. Note the position of the mutated Ala59. The orientation of the four figures is approximately the same. The $2F_{obs} - F_{calc}$ was contoured at the 1.0σ level.

Table 5
Solved X-ray structures of L-PGDS.

Mutant	C65A	C65A	C65A	C65A	C65A	Wild type (apo)	Wild type (co-crystals)
Species	Mouse	Mouse	Human	Human	Human	Human	Human
Space group	$P2_12_12_1$	$C222_1$	$P6_122$	$P4_1$	$P6_122$	$P2_12_12_1$	$P2_12_12_1$
Unit-cell parameters							
a (Å)	46.2	46.3	60.5	90.2	61.0	36.4	36.2
b (Å)	66.8	67.1	60.5	90.2	61.0	56.4	56.4
c (Å)	105.3	104.6	177.2	35.6	179.5	73.0	72.9
α (°)	90.0	90.0	90.0	90.0	90.0	90.0	90.0
β (°)	90.0	90.0	90.0	90.0	90.0	90.0	90.0
γ (°)	90.0	90.0	120.0	90.0	120.0	90.0	90.0
Molecules in the asymmetric unit	2	1	1	2	1	1	1
Resolution range (Å)	56.8–2.10	10.0–2.00	20.0–1.66	50.0–1.70	30.5–1.40	44.6–2.09	44.6–1.88
PDB code	2czt	2czu	3o19	3o2y	3o22	4imn	4imo
Reference	Kumasaka *et al.* (2009)	Kumasaka *et al.* (2009)	Zhou *et al.* (2010)	Zhou *et al.* (2010)	Zhou *et al.* (2010)	Lim *et al.* (2013)	Lim *et al.* (2013)

genous fatty acids observed by Zhou *et al.* (2010), so that the PEG–L-PGDS structure can be considered to be one of the holo structures of the enzyme.

The interaction of L-PGDS with PEG was confirmed by fluorometric titrations and isothermal titration calorimetry. After trying several alternatives, in both cases it was found that fitting of the data could be best performed assuming a stoichiometry of two protein molecules bound to a single PEG unit, in agreement with the crystallographic data.

Fig. 2(*b*) shows a representative fluorometric titration of a L-PGDS sample with the solution used to prepare crystal form 3. The figure represents the titration curves obtained with 0.5 µl injections of the crystallization solution. Every curve was normalized against a solution consisting of 20 m*M* Tris–HCl pH 7.5 (PGDS buffer) titrated with the same volume of crystallization solution. The arrow indicates the progressive quenching of the maximal fluorescence emission owing to the addition of PEG 4000 and the inset shows the fluorescence quenching as a function of PEG 4000 concentration, which can be used to obtain a K_d of 215 µ*M*.

Fig. 2(*c*) reports the experimental ITC data in a corrected heat rate *versus* time plot. The bottom of the figure shows the normalized fit assuming a stoichiometry of two L-PGDS molecules per PEG molecule (as observed in the crystals). The figure represents the titration curves obtained with 2 µl injections of a 9 µ*M* L-PGDS solution added to 300 µl of the diluted precipitating solution (750 µ*M* in PEG 4000). Analysis of the data yields a dissociation constant K_d of 210 µ*M*, which is in very good agreement with the fluorometric result. The apparent difference between the initial portion of the ITC and the fluorometric curves is simply owing to the use of larger aliquots of the titrant in fluorimetry, which was necessary to produce an observable signal.

3.3. The C65A/K59A double mutant

The C65A/K59A double mutant was prepared because mutation of Lys59, one of the few conserved charged residues in the external part of the ligand-binding cavity, to Ala was found to increase the catalytic efficiency of the enzyme (Zhou *et al.*, 2010), a fact that could be explained by its involvement in entrance/exit of the ligands to/from the cavity. A comparison of the position of this side chain in crystal forms 1 and 2 reveals that in the molecule bound to PEG the residue points towards the inside and is in close hydrophobic contact with the ligand, while in the apo forms it is found pointing towards the outside of the cavity. The double mutant was crystallized in three different space groups, crystal forms 4, 5 and 6, the first with no ligand in the cavity and the second and third with PEG bound. Although in the apo form of the double mutant the molecules pack differently from those of the single mutant C65A (crystal form 2), access to the cavity is equally impeded by the presence of lattice interactions with symmetry-related molecules in both molecules in the asymmetric unit. Fig. 3(*a*) compares the C_α chain trace of the apo forms of the C65A and C65A/K59A mutants. The single mutant is shown in blue and the double mutant is shown in red. The most noticeable differences are found in loop L1, which contains the first eight-amino-acid helix, and in the position of the side chains of Trp54 and Trp112, which are not in contact in the single mutant and become closer to each other in the double mutant, with their shortest distance changing from about 9 Å to about 4–5 Å. Since the packing of the molecules in the two different crystal forms involves these areas, these differences cannot be ascribed to the absence of the Lys chain in the cavity but might be owing to different packing in the two different space groups.

The chain traces of the single and double mutant bound to PEG are compared in Fig. 3(*b*), in which the double mutant is again shown in red while the single mutant is shown in green. Note that while the positions of the side chains of the two tryptophans in the figure, Trp54 and Trp112, are not very different in the single and double mutants, the ring of Phe143 in the double mutant points towards the interior of the cavity, probably to occupy space left vacant by the lysine side chain.

The electron density of the side chain of Lys59 is shown in Fig. 3(*c*) and it is found to be in close contact with the PEG molecule that curls around it. Fig. 3(*d*) shows the binding of

Table 6
Comparison of ligand-binding sites of L-PGDS mutants.

Mutant	Crystal form	Space group	Monomer	Ligand	Volume 1, *CASTp* (Å^3)	Volume 2, *CASTp* (Å^3)	Volume 1, *POCASA* (Å^3)
C65A	1	$P6_122$	*A*	PEG	461.2	4.5	446
C65A	2	*P*1	*A*	None	879.6	6.1	750
C65A	2	*P*1	*B*	None	606.8		852
C65A	3	$P4_1$	*A*	PEG	466.3	1.7	391
C65A	3	$P4_1$	*B*	PEG	430.8	2.2	469
C65A/K59A	4	$P2_12_12_1$	*A*	None	502.3	4.0	538
C65A/K59A	4	$P2_12_12_1$	*B*	None	500.7	2.9	499
C65A/K59A	5	$P4_1$	*A*	PEG	525.9	1.7	494
C65A/K59A	5	$P4_1$	*B*	PEG	313.9	1.6	542
C65A/K59A	6	$P4_1$	*A*	None	640.1	2.9	439
C65A/K59A	6	$P4_1$	*B*	None	332.7	1.8	419
C65A/K59A	6	$P4_1$	*C*	None	445.2	3.2	384
C65A/K59A	6	$P4_1$	*D*	None	501.8		441
C65A/K59A	6	$P4_1$	*E*	PEG	517.7	4.4	501
C65A/K59A	6	$P4_1$	*F*	PEG	548.1	4.1	477
C65A/K59A	6	$P4_1$	*G*	PEG	377.5	1.9	439
C65A/K59A	6	$P4_1$	*H*	PEG	563.8	2.3	490
C65A/W54F	7	*P*1	*A*	None	1060.2	0.7	920
C65A/W54F	7	*P*1	*B*	None	629.4	0.7	367
C65A/W112F	8	*P*1	*A*	None	860.1	1.1	605
C65A/W112F	8	*P*1	*B*	None	952.4	1.0	396
C65A/W54F/W112F	9	*P*1	*A*	None	891.5	0.6	732
C65A/W54F/W112F	9	*P*1	*B*	None	329.7	2.7	423

Table 7
Ligand-binding site volume and conserved water molecules of other L-PGDS structures.

Solvent-accessible volume of the binding cavity calculated with *CASTp* (Liang *et al.*, 1998) considering only protein atoms.

Mutant	Species	Space group	Monomer	Ligand	Volume 1 (Å^3)	Volume 2 (Å^3)	Conserved water molecules	PDB code
C65A	Mouse	$P2_12_12_1$	*A*	—	355.8	44.4	None	2czt
C65A	Mouse	$C222_1$	*A*	—	385.7	72.4	*A*190	2czu
C65A	Mouse	$C222_1$	*B*	—	465.8	76.7	*B*192	2czu
C65A	Human	$P6_122$	*A*	Fatty acids	324.6	4.6	*A*213	3o19
C65A	Human	$P4_1$	*A*	Fatty acids	458.4	0.4	*A*4	3o2y
C65A	Human	$P4_1$	*B*	Fatty acids	445.3	2.6	*B*200	3o2y
C65A	Human	$P6_122$	*A*	Fatty acids	429.9	6.9	*A*2	3o22
Wild type	Human	$P2_12_12_1$	*A*	PEG	588.2	0.8	*A*306	4imn
Wild type	Human	$P2_12_12_1$	*A*	Substrate analogue	1086.1	—	*A*310	4imo

PEG in the double mutant. The absence of contacts with the Lys gives more freedom of movement to the PEG molecule and thus less defined electron density is observed for the areas of the PEG molecule that were in contact with the Lys side chain. The orientation of the ligand is very similar in the single and double mutants. This additional freedom of movement is reflected by a slightly higher dissociation constant for the double mutant as determined by both fluorometric titrations and ITC. The first method yields a dissociation constant for the double mutant of $K_d = 321$ μM, whereas the second gives a K_d value of 297 μM.

3.4. Mutants with tryptophan replaced by phenylalanine

Two of the three Trp residues present in human prostaglandin D synthase are present at the entrance of the cavity that harbours the ligand-binding site and enzyme active site: Trp54 and Trp112. The third tryptophan, Trp43, is in β-strand A and has very clear electron density in the C65A mutant in an area on the surface of the molecule, and its plane is in hydrophobic contact with Phe39, which is more internal, and also with Arg51, which is more superficial. In the mutants in which the tryptophans at the entrance of the cavity were substituted by phenylalanines, the electron density of residue 43 is equally well defined. Phenylalanine was selected to replace the two tryptophans because it was assumed to be a less perturbing change from a structural point of view despite the fact that the two amino acids are known to behave quite differently (Braun & von Heijne, 1999).

Two double mutants, C65A/W54F and C65A/W112F, and a triple mutant with the two tryptophans replaced by two phenylalanines were prepared. The crystallographic data listed in Table 3 shows that the three crystal forms, although growing under different conditions, are virtually isomorphous. The three crystal forms are also closely related to crystal form 2, the apo form of the single mutant C65A. In fact, monomer *A* of crystal form 2 can be superimposed on monomer *A* of the triple mutant (crystal form 9) by the rotation $\alpha = -8.17^\circ$, $\beta = 1.90^\circ$, $\gamma = 8.92^\circ$ and the translation $x = -0.32$ Å, $y = -0.21$ Å, $z = 0.27$ Å. The ligand-binding site of these mutants is thus blocked by the packing of the molecules in the crystals, a fact that was confirmed by soaking experiments with several ligands.

The two tryptophans at the entrance to the cavity are found in loops L1 (Trp54) and L5 (Trp112) and the electron density of the phenyl rings is less well defined than that of the indole rings in the nonmutated structures. Interestingly, in the mutants in which only one phenylalanine was introduced the electron density of the remaining indole ring is also more poorly defined. Mutation of only one of the two tryptophans causes a displacement of both side chains and the final position adopted by the mutated phenylalanine ring and the nonmutated indole is very similar independently of which of the two residues was changed. Fig. 4(*a*) is a superposition of the C_α chain trace of the C65A mutant (green), the C65A/W54F double mutant (blue) and the C65A/W112F double mutant (red). Note that the ring of Phe143 remains in virtually the same position in all three mutants. Its electron density is very well defined in both the two double mutants and the triple mutant. Fig. 4(*b*) shows the superposition of the single C65A mutant and the triple C65A/W54F/W112F mutant. The

position of the two mutated phenylalanine rings is very similar to that adopted by the rings of the mutants in which only one tryptophan was changed.

4. Discussion

The space groups, resolutions and PDB codes of the crystal structures of lipocalin-type prostaglandin D synthase available to date are listed in Table 5. Two correspond to the wild-type human enzyme and the other five to the C65A mutant; the first two published were of the mouse enzyme and the other three are of the human enzyme bound to palmitic and oleic acid. All of the molecules that we have examined contain the C65A mutation, and in addition we have introduced mutations in other residues that are expected to play a role in the entrance/exit of the ligands to/from the cavity. Our crystal form 1 is very similar to crystal forms 1 and 3 of Zhou *et al.* (2010), but in our crystals L-PGDS does not have fatty acids bound but instead has PEG. Analogously, our crystal form 3 is very similar to crystal form 2 of Zhou *et al.* (2010) and again PEG occupies the place of the fatty acids. The apo form of this conformation is our crystal form 2, in which there is no ligand bound to the L-PGDS molecule and access to the cavity is prevented by the packing of the molecules in the crystals. Figs. 1(*c*) and 1(*d*) compare the two holo forms that we have examined with the apo form of the same single mutant. The holo forms in the two crystals are very similar to one another and differ from the apo form in loop L1, in which the first helix in the molecule is less structured and shorter in the apo form.

The solvent-accessible volume of the ligand-binding cavity of all of the molecules present in the nine crystal forms that we have studied were calculated with *CASTp* (Liang *et al.*, 1998) and *POCASA* (Yu *et al.*, 2010). The results of these calculations are listed in Table 6 for the structures that we present here. As the table shows, the values obtained with the two methods do not always correlate completely. The first program identified a larger more external and a smaller more internal cavity in most cases. The definition of the two cavities corresponds to those in mouse L-PGDS and the five hydrophobic amino acids that were identified to separate them (Kumasaka *et al.*, 2009) are conserved in the sequence of the human protein. Four of the five residues, Leu96, Val118, Leu131 and Tyr149, superimpose quite well, while the fifth, Leu79, points more towards the interior of the second cavity in human L-PGDS. The results in the table indicate that the packing of the molecules influences the accessible volume and the two members of an asymmetric unit of the apo forms (crystal forms 2, 7, 8 and 9) do not show comparable values. There is a substantial variability in the different crystals, but in general it can be said that the holo forms tend to have smaller cavity volumes, suggesting that the protein tends to establish tight contacts with the ligand. Although the volume of the cavities of the apo forms of the mutants varies substantially depending on the position of the molecule in the crystal lattice and the variable position of the loops at the entrance, in general the cavities of the apo forms are somewhat larger than those of the protein bound to PEG.

Fig. 5(*a*) shows a stereo diagram of three models with different cavity volumes superimposed. The models are those of the apo and holo forms of the C65A/K59A double mutant and the apo form of the C65A/W54F double mutant, which

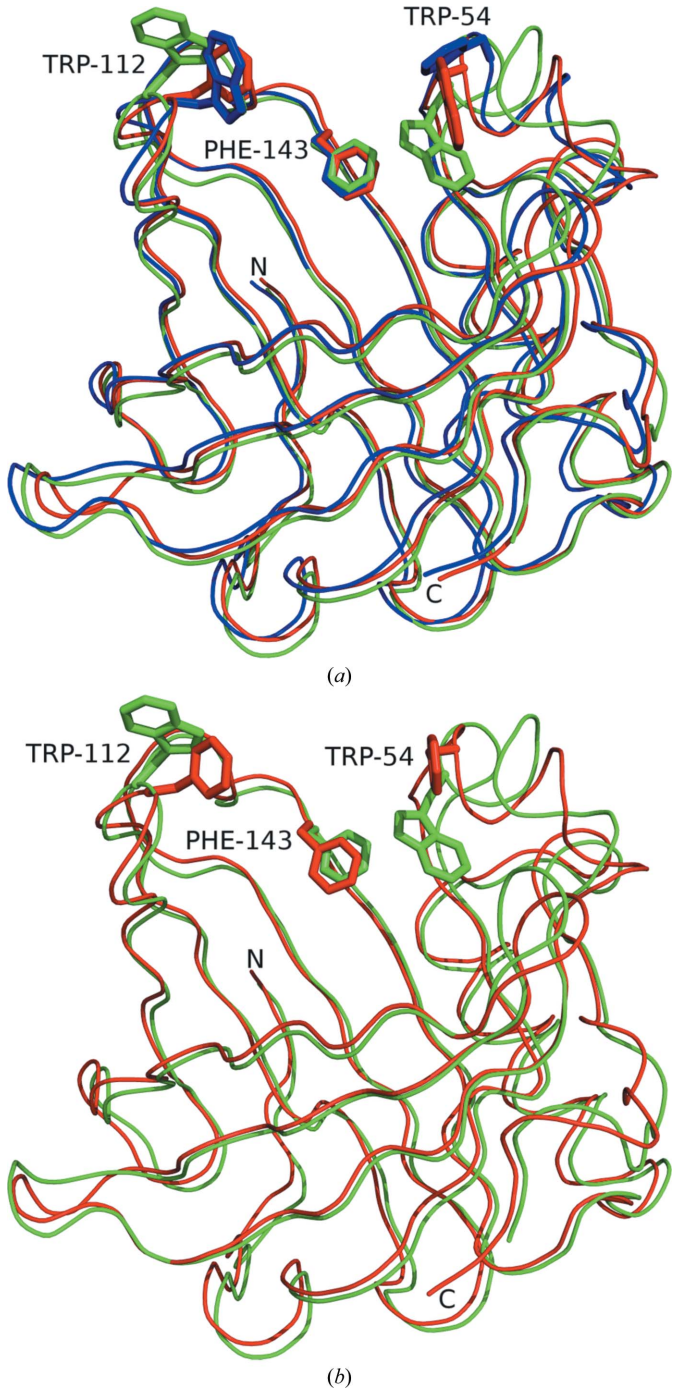

Figure 4
Mutants with tryptophan replaced by phenylalanine. (*a*) Superposition of the C_α chain traces of the C65A mutant (green, crystal form 2), the C65A/W54F double mutant (blue, crystal form 7) and the C65A/W112F double mutant (red, crystal form 8). Note that the ring of Phe143 remains in virtually the same position in all three mutants. (*b*) Superposition of the C_α chain traces of the C65A mutant (green, crystal form 2) and the triple mutant C65A/W54F/W112F (red, crystal form 9). The position of the two mutated phenylalanine rings is the same as that adopted by the rings of the mutants in which only one tryptophan was changed.

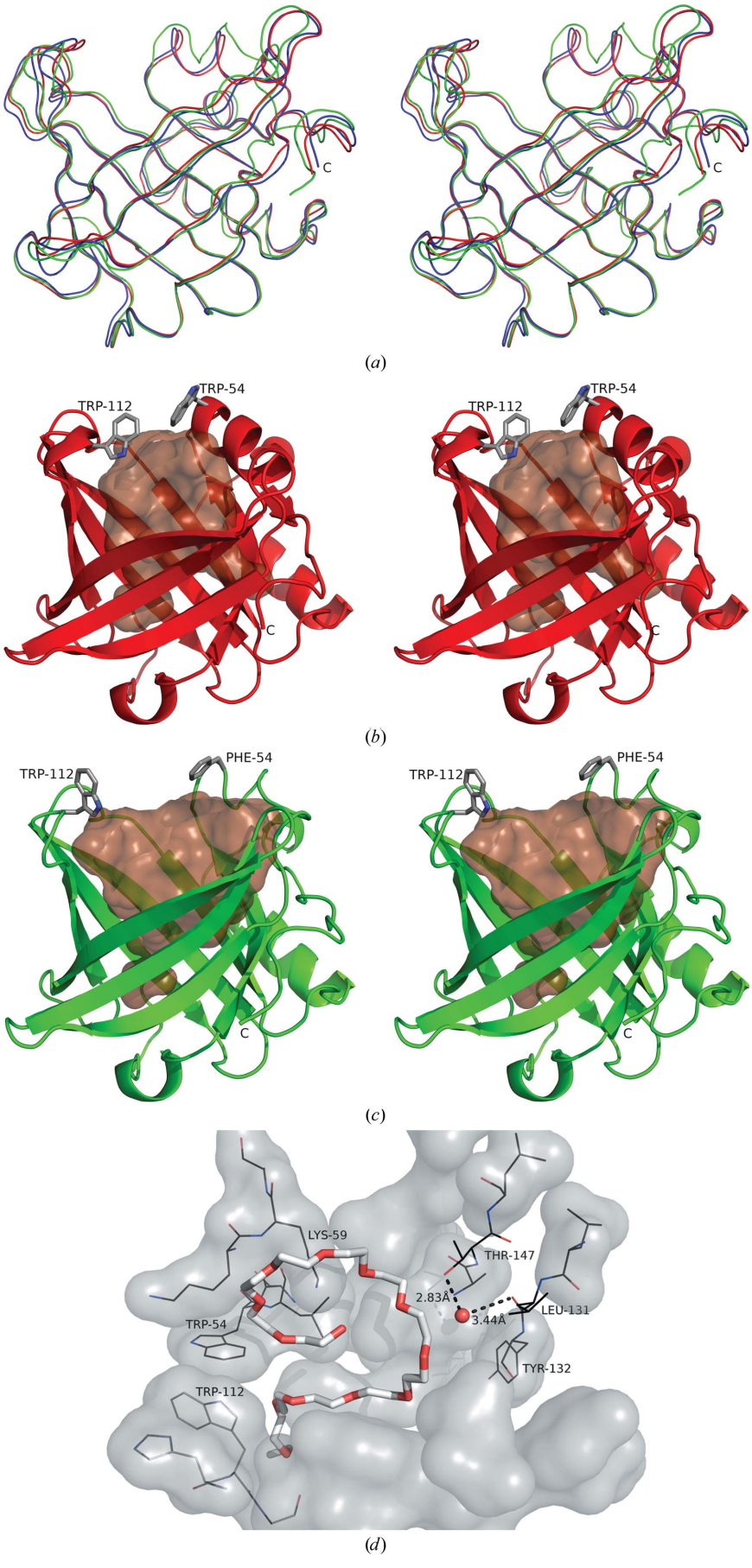

has the largest cavity volume (Table 6). Figs. 5(*b*) and 5(*c*) represent the smallest and the largest cavity volumes as contact surfaces defined as indicated in the figure caption. The holo form of the C65A/K59A mutant is shown in red (Fig. 5*b*) and the apo form of the C65A/W54F double mutant is shown in green (Fig. 5*c*).

In agreement with our results, small-angle X-ray scattering (SAXS) experiments with the apo form of the C65A mutant of mouse L-PGDS and its complexes with hydrophobic ligands have shown that the binding of a lipophilic ligand induces a reduction of the radius of gyration in the holo form of the enzyme; this is in contrast to the radii of gyration of β-lactoglobulin and retinol-binding protein, which remain almost the same before and after ligand binding (Inoue *et al.*, 2009). The important influence of the packing in the crystals on the cavity volume is also shown by the variability observed in the eight molecules present in the asymmetric unit of crystal form 6. In this crystal form, which diffracted to a somewhat lower resolution, the electron density of the ligands was not as clear as in the other forms and therefore a model for PEG was included in only four of the eight molecules in the asymmetric unit: *E*, *F*, *G* and *H*.

Mutation of either one or two tryptophans at the entrance of the cavity does not appear to substantially change the volumes

Figure 5
The ligand-binding cavity in the mutants. (*a*) Stereo diagram showing three models with different cavity volumes superimposed. The models are those of the double mutant holo C65A/K59A (monomer *B*, crystal form 5, red, volume 1 = 313.9 Å^3, volume 2 = 1.6 Å^3), the apo C65A/K59A mutant (monomer *A*, crystal form 4, blue, volume 1 = 502.3 Å^3, volume 2 = 4.0 Å^3) and the C65A/W54F double mutant (monomer *A*, crystal form 7, green, volume 1 = 1060.2 Å^3, volume 2 = 0.7 Å^3). (*b*) Stereo diagram showing the cavity of the double mutant holo C65A/K59A (monomer *B*, crystal form 5). The transparent orange surface represents the approximate size of the internal cavity, 313.9 + 1.6 Å^3, defined by a sphere of 1.4 Å radius. (*c*) Stereo diagram showing the cavity of the double mutant apo C65A/W54F (monomer *A*, crystal form 7). The transparent surface represents the approximate size of the internal cavity, 1060.2 Å^3, defined by a sphere of 1.4 Å radius. (*d*) Surface representation of the ligand-binding cavity of the C65A mutant of human L-PGDS. The figure was prepared with the coordinates of the holo form in crystal form 1. PEG and the conserved water molecule are shown in the picture together with the amino acids that are closest to them.

of the cavities since, as pointed out above, changing one tryptophan alters the position of the other and the final position of the new phenylalanines is virtually the same regardless of whether or not the other tryptophan is mutated.

The main conclusion that can be drawn from similar calculations for the crystal forms in Table 7 is that the ligand cavity of mouse L-PGDS appears to be somewhat smaller than that of the human counterpart, whereas the second, more internal, cavity is larger in the mouse enzyme. The two main factors that explain why the second cavity is smaller in the human protein are the position of Leu79, which points towards the second cavity in human L-PGDS, and the position of the side chain of Phe39, which points towards the interior of the cavity in human L-PGDS and is more superficial in mouse L-PGDS.

Examination of Table 3 shows that a total of 23 protein molecules are present in the asymmetric units of the nine crystal forms of the different mutants and that the resolution of the data is sufficiently high to justify analysis of the position of the water molecules in the cavities. When this is performed it is found that there is one water molecule in approximately the same position in virtually all of the available protein cavities, with the exception of three monomers in crystal form 6, in which fewer solvent molecules were identified because of the significantly lower resolution of the data. It has been labelled *A*501 in PDB entry 4orr.

Comparison of the location of this water molecule with those in the other structures of L-PGDS listed in Table 5 reveals that the same position is occupied by water in all of the human L-PGDS structures and in one of the mouse L-PGDS structures. The molecule has been identified in Table 7, in which the cavity volumes of the available structures calculated with *CASTp* are also given.

The published crystal structures of H-PGDS show that there are two water molecules located at the active site, one of which is in proximity to Thr159 and Leu199; it coordinates with inhibitors of the enzyme and appears to be in a position that precludes replacement by an inhibitor atom (Trujillo *et al.*, 2012). The position of the conserved water molecule in L-PGDS is shown in Fig. 5(*d*), which also gives the distances to the OG atom of Thr147 and the O atom of Leu131. This figure, which was prepared with the coordinates of the holo form in crystal form 1, also shows the PEG molecule and suggests a situation quite similar to that described for H-PGDS. Thus, in spite of the fact that H-PGDS and L-PGDS have very different three-dimensional structures and do not show any sequence similarity, a conserved water molecule is found in the proximity of two identical amino acids that coordinate the solvent molecule in a very similar way.

To summarize, we can say that the holo forms (bound to PEG) of the C65A mutant of human L-PGDS and of the double mutant C65A/K59A are more compact than the apo forms, a fact that may be attributed to conformational flexibility of the L-PGDS molecule, which is probably required by the high versatility of the binding properties of the protein.

Examination of the apo forms of the double mutants C65A/W54F and C65A/W112F and the triple mutant C65A/W54F/W112F has revealed that mutation of one or both tryptophans induces a similar displacement in the position of both side chains, Trp54 and Trp112. In addition, we note that mutation of Lys59 does not seem to affect the binding of PEG to the ligand-binding cavity.

Taken together, our observations indicate that the residues that we have mutated indeed appear to play a role in the entrance/exit process of the substrate and/or other ligands into/out of the binding cavity of the lipocalin. The role of a conserved water molecule in the ligand-binding cavity identified in this study deserves further exploration.

We thank Guillermo Montich for helpful discussions and the staff of the ESRF in Grenoble (Proposal MX 1552) for assistance during data collection. The coordinates of the models and the structure factors of all of the crystal forms have been deposited in the Protein Data Bank. The PDB accession codes are given in Table 3. This work was supported by Fondazione Cassa di Risparmio di Verona, Vicenza, Belluno e Ancona.

References

Adams, P. D. *et al.* (2010). *Acta Cryst.* D**66**, 213–221.
Afonine, P. V., Grosse-Kunstleve, R. W. & Adams, P. D. (2005). *CCP4 Newsl. Protein Crystallogr.* **42**, contribution 8.
Bachmann, G., Petereit, H., Djenabi, U. & Michel, O. (2002). *Neurosurgery*, **50**, 571–576.
Beuckmann, C. T., Aoyagi, M., Okazaki, I., Hiroike, T., Toh, H., Hayaishi, O. & Urade, Y. (1999). *Biochemistry*, **38**, 8006–8013.
Beuckmann, C. T., Lazarus, M., Gerashchenko, D., Mizoguchi, A., Nomura, S., Mohri, I., Uesugi, A., Kaneko, T., Mizuno, N., Hayaishi, O. & Urade, Y. (2000). *J. Comp. Neurol.* **428**, 62–78.
Braun, P. & von Heijne, G. (1999). *Biochemistry*, **38**, 9778–9782.
Davis, I. W., Leaver-Fay, A., Chen, V. B., Block, J. N., Kapral, G. J., Wang, X., Murray, L. W., Arendall, W. B. III, Snoeyink, J., Richardson, J. S. & Richardson, D. C. (2007). *Nucleic Acids Res.* **35**, W375–W383.
Eguchi, N., Minami, T., Shirafuji, N., Kanaoka, Y., Tanaka, T., Nagata, A., Yoshida, N., Urade, Y., Ito, S. & Hayaishi, O. (1999). *Proc. Natl Acad. Sci. USA*, **96**, 726–730.
Emsley, P., Lohkamp, B., Scott, W. G. & Cowtan, K. (2010). *Acta Cryst.* D**66**, 486–501.
Evans, P. (2006). *Acta Cryst.* D**62**, 72–82.
Flanagan, J. U. & Smythe, M. L. (2011). *Drug Metab. Rev.* **43**, 194–214.
Flower, D. R., North, A. C. T. & Sansom, C. E. (2000). *Biochim. Biophys. Acta*, **1482**, 9–24.
Garza, L. A., Liu, Y., Yang, Z., Alagesan, B., Lawson, J. A., Norberg, S. M., Loy, D. E., Zhao, T., Blatt, H. B., Stanton, D. C., Carrasco, L., Ahluwalia, G., Fischer, S. M., FitzGerald, G. A. & Cotsarelis, G. (2012). *Sci. Transl. Med.* **4**, 126–134.
Hoffmann, A., Conradt, H. S., Gross, G., Nimtz, M., Lottspeich, F. & Wurster, U. (1993). *J. Neurochem.* **61**, 451–456.
Inoue, K., Yagi, N., Urade, Y. & Inui, T. (2009). *J. Biochem.* **145**, 169–175.
Jordan, W., Tumani, H., Cohrs, S., Eggert, S., Rodenbeck, A., Brunner, E., Rüther, E. & Hajak, G. (2004). *Sleep*, **27**, 867–874.
Jowsey, I. R., Thomson, A. M., Flanagan, J. U., Murdock, P. R., Moore, G. B. T., Meyer, D. J., Murphy, G. J., Smith, S. A. & Hayes, J. D. (2001). *Biochem. J.* **359**, 507–516.
Kanaoka, Y., Ago, H., Inagaki, E., Nanayama, T., Miyano, M., Kikuno, R., Fujii, Y., Eguchi, N., Toh, H., Urade, Y. & Hayaishi, O. (1997). *Cell*, **90**, 1085–1095.

Kanaoka, Y. & Urade, Y. (2003). *Prostaglandins Leukot. Essent. Fatty Acids*, **69**, 163–167.
Kanekiyo, T., Ban, T., Aritake, K., Huang, Z.-L., Qu, W.-M., Okazaki, I., Mohri, I., Murayama, S., Ozono, K., Taniike, M., Goto, Y. & Urade, Y. (2007). *Proc. Natl Acad. Sci. USA*, **104**, 6412–6417.
Krissinel, E. & Henrick, K. (2004). *Acta Cryst.* D**60**, 2256–2268.
Kumasaka, T., Aritake, K., Ago, H., Irikura, D., Tsurumura, T., Yamamoto, M., Miyano, M., Urade, Y. & Hayaishi, O. (2009). *J. Biol. Chem.* **284**, 22344–22352.
Kume, S., Lee, Y.-H., Miyamoto, Y., Fukada, H., Goto, Y. & Inui, T. (2012). *Biochem. J.* **446**, 279–289.
Kuruvilla, A. P., Hochwald, G. M., Ghiso, J., Castaño, E. M., Pizzolato, M. & Frangione, B. (1991). *Brain Res.* **565**, 337–340.
Laskowski, R. A., MacArthur, M. W., Moss, D. S. & Thornton, J. M. (1993). *J. Appl. Cryst.* **26**, 283–291.
Leslie, A. G. W. & Powell, H. R. (2007). *Evolving Methods for Macromolecular Crystallography*, edited by R. J. Read & J. L. Sussman, pp. 41–51. Dordrecht: Springer.
Liang, J., Edelsbrunner, H. & Woodward, C. (1998). *Protein Sci.* **7**, 1884–1897.
Lim, S. M., Chen, D., Teo, H., Roos, A., Jansson, A. E., Nyman, T., Trésaugues, L., Pervushin, K. & Nordlund, P. (2013). *J. Lipid Res.* **54**, 1630–1643.
Murshudov, G. N., Skubák, P., Lebedev, A. A., Pannu, N. S., Steiner, R. A., Nicholls, R. A., Winn, M. D., Long, F. & Vagin, A. A. (2011). *Acta Cryst.* D**67**, 355–367.
Peitsch, M. C. & Boguski, M. S. (1991). *Trends Biochem. Sci.* **16**, 363.
Pinzar, E., Miyano, M., Kanaoka, Y., Urade, Y. & Hayaishi, O. (2000). *J. Biol. Chem.* **275**, 31239–31244.
Qu, W.-M., Huang, Z.-L., Xu, X.-H., Aritake, K., Eguchi, N., Nambu, F., Narumiya, S., Urade, Y. & Hayaishi, O. (2006). *Proc. Natl Acad. Sci. USA*, **103**, 17949–17954.
Samy, E. T., Li, J. C. H., Grima, J., Lee, W. M., Silvestrini, B. & Cheng, C. Y. (2000). *Endocrinology*, **141**, 710–721.
Shimamoto, S., Yoshida, T., Inui, T., Gohda, K., Kobayashi, Y., Fujimori, K., Tsurumura, T., Aritake, K., Urade, Y. & Ohkubo, T. (2007). *J. Biol. Chem.* **282**, 31373–31379.
Sumathi, K., Ananthalakshmi, P., Roshan, M. N. A. M. & Sekar, K. (2006). *Nucleic Acids Res.* **34**, W128–W132.
Tanaka, R., Miwa, Y., Mou, K., Tomikawa, M., Eguchi, N., Urade, Y., Takahashi-Yanaga, F., Morimoto, S., Wake, N. & Sasaguri, T. (2009). *Biochem. Biophys. Res. Commun.* **378**, 851–856.
Tanaka, T., Urade, Y., Kimura, H., Eguchi, N., Nishikawa, A. & Hayaishi, O. (1997). *J. Biol. Chem.* **272**, 15789–15795.
Trujillo, J. I., Kiefer, J. R., Huang, W., Day, J. E., Moon, J., Jerome, G. M., Bono, C. P., Kornmeier, C. M., Williams, M. L., Kuhn, C., Rennie, G. R., Wynn, T. A., Carron, C. P. & Thorarensen, A. (2012). *Bioorg. Med. Chem. Lett.* **22**, 3795–3799.
Urade, Y. & Eguchi, N. (2002). *Prostaglandins Other Lipid Mediat.* **68–69**, 375–382.
Urade, Y. & Hayaishi, O. (2000). *Biochim. Biophys. Acta*, **1482**, 259–271.
Urade, Y., Tanaka, T., Eguchi, N., Kikuchi, M., Kimura, H., Toh, H. & Hayaishi, O. (1995). *J. Biol. Chem.* **270**, 1422–1428.
Vagin, A. & Teplyakov, A. (2010). *Acta Cryst.* D**66**, 22–25.
Winn, M. D. *et al.* (2011). *Acta Cryst.* D**67**, 235–242.
Yu, J., Zhou, Y., Tanaka, I. & Yao, M. (2010). *Bioinformatics*, **26**, 46–52.
Zhou, Y., Shaw, N., Li, Y., Zhao, Y., Zhang, R. & Liu, Z.-J. (2010). *FASEB J.* **24**, 4668–4677.